ACS Macro Letters

Letter

pubs.acs.org/macroletters

Tunable Film Morphologies of Brush–Linear Diblock Copolymer Bearing Difluorene Moieties Yield a Variety of Digital Memory Properties

Byungcheol Ahn,[†,∥] Dong Min Kim,[†,∥] Jung-Ching Hsu,[‡,∥] Yong-Gi Ko,[†] Tae Joo Shin,[§] Jehan Kim,[§] Wen-Chang Chen,*[,‡] and Moonhor Ree*[,†]

[†]Department of Chemistry, Division of Advanced Materials Science, Center for Electro-Photo Behaviors in Advanced Molecular Systems, Pohang Accelerator Laboratory, Polymer Research Institute, and BK School of Molecular Science, Pohang University of Science & Technology, Pohang 790-784, Republic of Korea

[‡]Department of Chemical Engineering and Institute of Polymer Science and Engineering, National Taiwan University, Taipei 106, Taiwan

[§]Pohang Accelerator Laboratory, Pohang University of Science & Technology, Pohang 790-784, Republic of Korea

Supporting Information

ABSTRACT: An amphiphilic brush–linear diblock copolymer bearing a rigid difluorene moiety was synthesized, yielding a copolymer with a high thermal stability and excellent processability. The immiscibility of the blocks induced the formation of a variety of nanostructures, depending on the fabrication conditions, which differed significantly from the nanostructures observed among common diblock copolymers in similar composition. Interestingly, the orientations of the nanostructures could be controlled. The nanostructured polymer displayed a variety of tunable morphologies that yielded distinct electrical memory properties when incorporated as the active layer into a digital memory device. The memory devices could be operated under very low power consumption levels and displayed excellent unipolar switching properties.

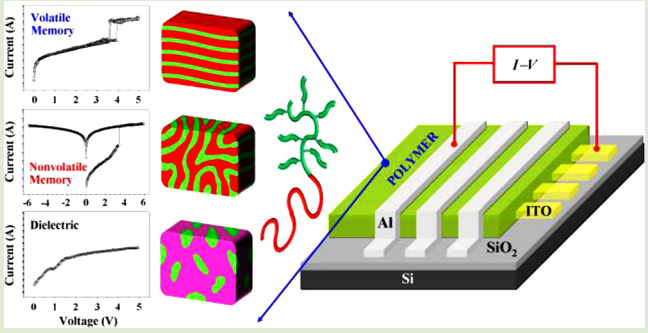

Block copolymers have received attention for their ability to form a variety of phase-separated morphologies, depending on the block components, composition, and molecular weight.[1,2] Block copolymers can be designed to include specific functionalities that are desirable for applications in advanced technology fields, such as microelectronics, electro-optics, displays, and biomaterials. To this end, a significant effort has been applied toward incorporating functional moieties into the backbones and/or side groups of block copolymers.[3−8] Several block copolymers bearing π-conjugated units, such as fluorine, thiophene, and phenylene, have been synthesized and examined for their utility in light-emitting diode and photovoltaic device applications.[4,6−8] The charge transport properties among π-conjugated moieties in block copolymer systems suggest that such systems would be useful as electrically active materials in high-performance memory devices. They may have significant advantages over inorganic silicon- and metal-oxide-based memory materials in that their dimensions can easily be miniaturized and their properties can easily be tailored through chemical synthesis as well as nanostructure formation. However, block copolymers have not yet been tested in electrical memory devices. The film performance can be sensitive to the morphological structures resulting from phase separation among immiscible block components. Variations in the fabrication conditions can also influence the morphological structures. Thus, there is a need in the field to examine the factors that determine the morphological structures of block copolymer films and the relationship between the structures and the electrical memory device performances.

In this study, we synthesized an amphiphilic poly(4-di(9,9-dihexylfluoren-2-yl)styrene)-*b*-poly(2-vinylpyridine) (PStFl2$_m$-*b*-P2VP$_n$) where one block included difluorene moieties: PStFl2$_7$-*b*-P2VP$_{121}$ (29/71, v/v; 17900 $\bar{M}_n$ (number-average molecular weight); 1.080 PDI (polydispersity index)) (Figure 1A). For this dilock copolymer, we attempted to investigate the morphologies of the nanoscale thin films and the electrical memory device characteristics.

The thermogravimetry analysis found that the brush–linear PStFl2$_7$-*b*-P2VP$_{121}$ copolymer is thermally stable up to around 350 °C. The highest occupied molecular orbital (HOMO) and lowest unoccupied molecular orbital (LUMO) levels were determined to be −5.79 and −2.55 eV, respectively, which are

Received: April 30, 2013
Accepted: June 5, 2013
Published: June 6, 2013

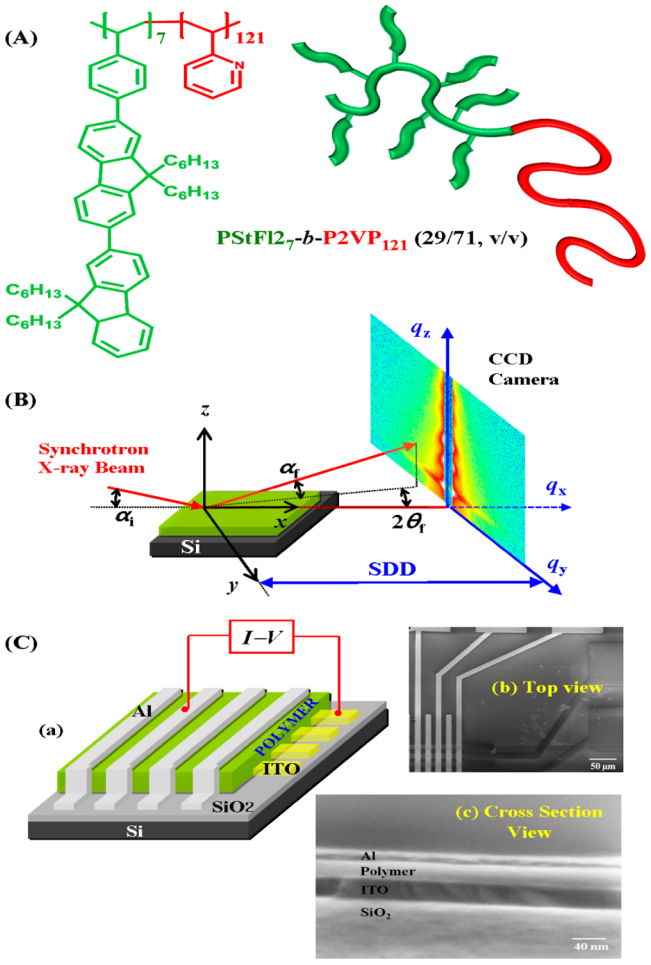

Figure 1. (A) Chemical structure of PStFl2$_7$-*b*-P2VP$_{121}$ copolymer. (B) Geometry of GIXS: α_i is the incident angle at which the X-ray beam impinges on the film surface; α_f and $2\theta_f$ are the out-of-plane and in-plane exit angles of the out-going X-ray beam respectively, and q_x, q_y, and q_z are the components of the scattering vector **q**. (C) Memory device fabricated with PStFl2$_7$-*b*-P2VP$_{121}$ and Al top and ITO bottom electrodes: (a) schematic diagram; (b, c) scanning electron microscopy (SEM) images.

similar to those ofthe PStFl2 homopolymer (Figures S1 and S2 in the Supporting Information). Synchrotron grazing incidence X-ray scattering (GIXS) measurements of the block copolymer were conducted to obtain structural information about the nanoscale thin films (Figure 1B). The diblock copolymer films, as well as the PStFl2 homopolymer films, revealed featureless grazing incidence wide-angle X-ray scattering (GIWAXS) patterns, regardless of the application of solvent annealing, thermal annealing, or a combination of the two types of annealing. Only one weak broad scattering ring around 16.70° was observed (Figure S3, Supporting Information). This ring was a typical amorphous halo ring, and its *d*-spacing was estimated to be 0.48 nm. The amorphous properties of the PStFl2 and P2VP homopolymers in the thin films yielded a featureless grazing incidence small-angle X-ray scattering (GISAXS) pattern. However, the diblock copolymer in films yielded a variety of featured GISAXS patterns depending on the film preparation conditions, indicative of the formation of domains of the blocks via phase separation due to the immiscibility between the blocks.

The as-cast film showed a faint scattering signal around the reflected X-ray beam position (Figure 2a). A weak broad

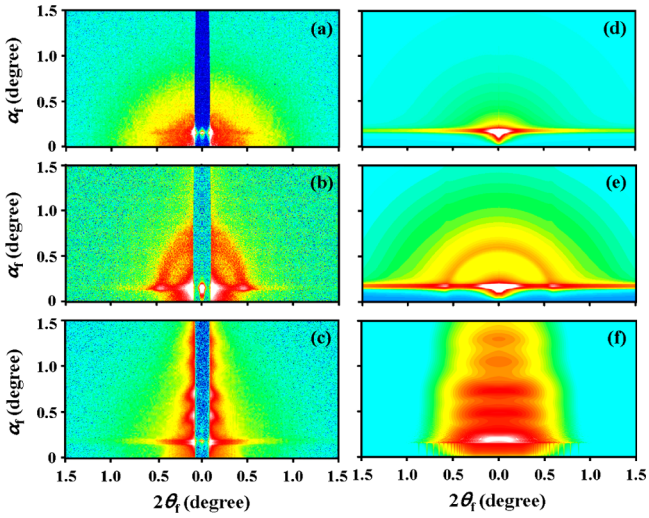

Figure 2. 2D GISAXS patterns of PStFl2$_7$-*b*-P2VP$_{121}$ copolymer films (100 nm) deposited on silicon substrates, measured at room temperature: (a, d) as-cast film (α_i = 0.164°); (b, e) film annealed under CB vapor for 1 h (α_i = 0.157°); (c, f) film annealed under CS_2 vapor for 1 h (α_i = 0.196°). Here, the scattering patterns in a–c are the experimental data, and those in d–f are the scattering images reconstructed from the structural parameters in Table 1 using the GIXS formulas.

scattering peak appeared in the in-plane scattering profile around 0.470°; however, the out-of-plane scattering profile was featureless (Figures 3a and b). The featured in-plane scattering profile could be satisfactorily fitted using the GIXS formula derived for a random two-phase domain (i.e., sea-and-island) structural model (Figure 4a; the derivation of the GIXS formula in the Supporting Information). These results indicated that a sea-and-island structure formed in the as-cast film, confirming that the two block components underwent phase separation; however, the phase separation was very limited through the film formation process. The PStFl2 domains formed with a very low population had an average size of 11.8 nm (Table 1). Taking these results into account, some of the as-cast films were further thermally annealed at various temperatures up to 200 °C to produce featured scattering patterns. However, thermal annealing failed to promote development of a defined nanostructure in the films.

Unlike the as-cast and thermally annealed films, the films annealed at room temperature under chlorobenzene (CB) vapor for 1 h displayed a clearly featured scattering pattern (Figure 2b). A strong scattering spot appeared at $2\theta_f$ = 0.457° and α_f = 0.140° (where $2\theta_f$ and α_f are the in-plane and out-of-plane scattering angles, respectively), and this spot was linked with a weak broad scattering ring. The in-plane scattering profile clearly revealed a scattering spot centered at 0.457°; above 1.0°, the scattering intensity decayed inversely with the 1.8th order of the scattering vector (Figure 3c). The out-of-plane scattering profile displayed a much broader weak scattering peak at 0.670° (Figure 3d). The broader peak was attributed to the partial overlap between the scattering features along the α_f direction from the reflected and transmitted X-ray beams, which is a feature of the GISAXS measurements gathered at the chosen grazing incidence angle α_i (0.157°). The

dx.doi.org/10.1021/mz4002113 | *ACS Macro Lett.* 2013, 2, 555–560

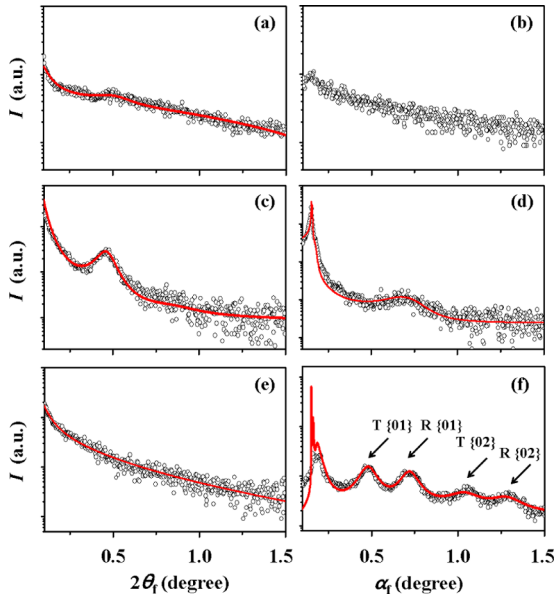

Figure 3. In-plane and out-of-plane scattering profiles extracted from the 2D GISAXS patterns in Figures 2a–c: (a) and (b) scattering profiles of the as-cast film extracted along the $2\theta_f$ direction at α_f = 0.150° and along the α_f direction at $2\theta_f$ = 0.460°, respectively; (c) and (d) scattering profiles of the CB-annealed film, extracted along the $2\theta_f$ direction at α_f = 0.140° and along the α_f direction at $2\theta_f$ = 0.120°, respectively; (e) and (f) scattering profiles of the CS_2-annealed film, extracted along the $2\theta_f$ direction at α_f = 0.200° and along the α_f direction at $2\theta_f$ = 0.080°, respectively. The black symbols are the measured data, and the red solid lines were obtained by fitting the data using the GIXS formulas.

featured in-plane and out-of-plane scattering profiles could be satisfactorily fitted using the GIXS formula derived for a lamellar structural model (Figures 3c–d; the GIXS formula derivation in Supporting Information). The obtained structural parameters are listed in Table 1. The GISAXS analysis confirmed that a lamellar structure was formed in the CB-annealed film, with a long period L of 14.6 nm, which consisted of a 5.0 nm thick PStFl2 layer h_{PStFl2} and a 9.6 nm thick P2VP layer h_{P2VP}, arranged in alternating stacks. However, the orientations of the lamellae were widely distributed. The second-order orientation factor O_s was only 0.261; the mean polar angle $\overline{\varphi}$ between the orientation vector **n** and the out-of-plane direction of the film was 0°, but the standard deviation σ_φ was very large, 76.0°. The positional distortion factor g was relatively high (0.210).

The diblock copolymer film annealed at room temperature under carbon disulfide (CS_2) vapor for 1 h displayed a featured scattering pattern (Figure 2c). The in-plane scattering profile was featureless (Figure 3e). By contrast, the out-of-plane scattering profile revealed several peaks (Figure 3f). The peaks at 0.480° and 1.060° were identified to be scattering features produced by the transmitted X-ray beam. These peaks were positioned relative to the specular reflections of 1 and 2, whereas the peaks at 0.720° and 1.300° were identified as scattering peaks from the reflected X-ray beam, which were positioned relative to the specular reflections of 1 and 2. The in-plane and out-of-plane scattering profiles could be satisfactorily fitted using the GIXS formula derived for a lamellar structural model (Figures 3e,f). The obtained structural parameters are listed in Table 1. These scattering analysis results collectively indicated that in the CS_2-annealed film the lamellar structures were well developed, and the lamellae were stacked along a direction normal to the film plane. The lamellar structure was characterized by L = 13.5 nm and consisted of a 4.6 nm thick PStFl2 layer h_{PStFl2} and a 8.9 nm thick P2VP layer h_{P2VP}, arranged in alternating stacks. The lamellar structure was characterized by O_s = 0.985 ($\overline{\varphi}$ = 0° and σ_φ = 5.5°) with respect to the out-of-plane direction of the film. The positional distortion factor g was very low (0.071). Overall, the lamellar structure formed in the CS_2-annealed film was much more ordered and preferentially oriented, compared to that of the CB-annealed film.

Surprisingly the lamellar structures observed above are quite different from cylinder structures observed for common flexible diblock copolymers in the same or similar volume fraction. Such lamellar structure formation might be attributed to the rigid chain nature of the PStFl2 block due to the difluorene unit, which can influence the phase diagram.

The structural parameters in Table 1 were used to reconstruct 2D GSAXS images. The reconstructed scattering images are displayed in Figures 2d–f and agreed well with the experimental data. Phase-separated structural models were proposed for the as-cast and solvent-annealed films based on the analysis results, as shown in Figures 4a–c.

The CS_2-annealed film was further investigated during heating at 300 °C and subsequent cooling using in situ GISAXS analysis, to characterize the structural stability and to identify any possible phase transitions. During the heating run, the scattering pattern varied very little in its intensity and shape at temperatures up to 130 °C; however, above 130 °C, the scattering pattern intensity weakened and then disappeared completely around 185 °C (Figure S4, Supporting Information). These scattering results indicated that the lamellar structure in the diblock copolymer film was thermally stable up to 130 °C (higher than the glass transition T_g (92 °C) of the P2VP phase), after which temperature the film structure degraded until reaching a completely disordered state at 185 °C. Such a limited structural stability of the lamellae was attributed to the relatively high thermal expansivity (i.e., high chain mobility) of the P2VP block phase at temperatures beyond 130 °C (Table 1). Once the lamellar structure had been destroyed, it could not be recovered through subsequent cooling (Figure S5, Supporting Information), further supporting the observation that thermal annealing did not promote the development of a lamellar structure in the diblock copolymer film.

In view of the above property and morphology characteristics, devices with a bottom electrode (indium–tin-oxide (ITO) or gold (Au))/polymer/top electrode (aluminum (Al)) sandwich structure (Figure 1C) were fabricated with the diblock copolymer or its homopolymers, and the electrical properties of the devices were evaluated. A range of very interesting memory properties were observed in the devices fabricated using 30 nm thick $PStFl2_7$-b-$P2VP_{121}$ films, depending on the film formation history. As shown in Figures 4d,e, the as-cast film always displayed a high resistance state during the positive and negative voltage sweeps, with a current compliance of 0.01 A, even though the current level increased slightly with increasing voltage, as observed in the P2VP homopolymer films (Figure S6a, Supporting Information). The CB-annealed film exhibited unipolar write-once-read-many-times (WORM) memory behavior, namely, permanent memory behavior (Figures 4f,g), as observed in the PStFl2 homopolymer film (Figure S6b, Supporting Information). The permanent memory

dx.doi.org/10.1021/mz4002113 | ACS Macro Lett. 2013, 2, 555–560

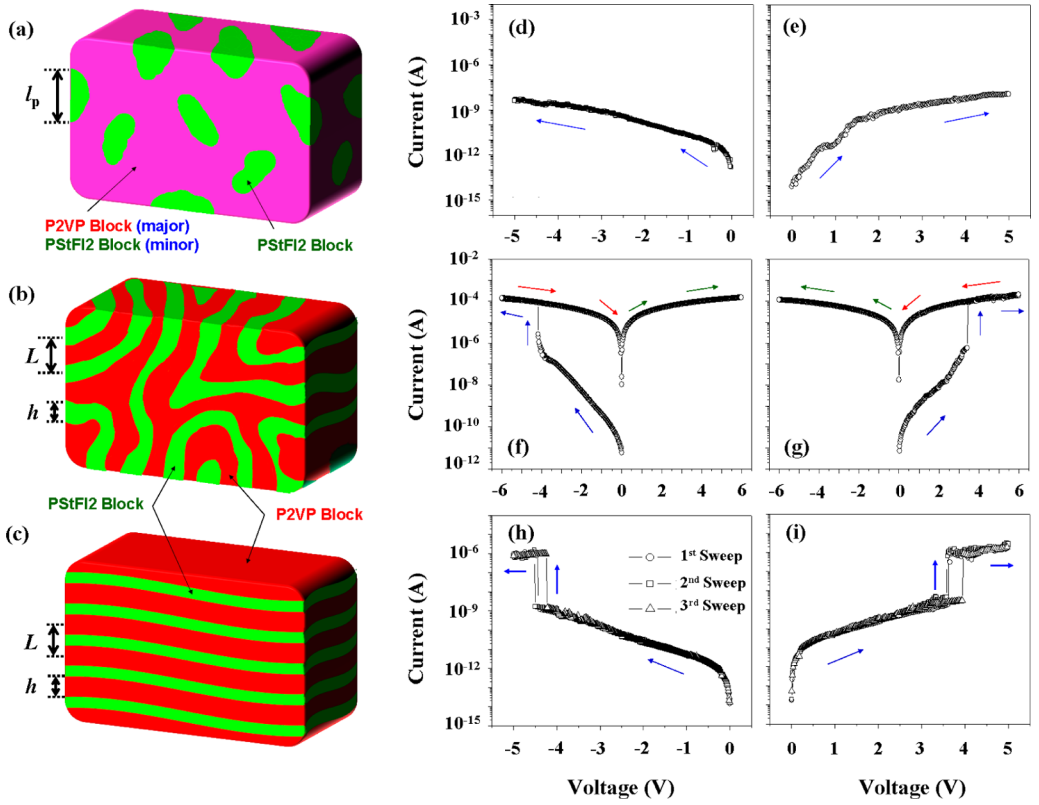

Figure 4. Schematic representations of the phase-separated nanostructures in the PStFl2$_7$-*b*-P2VP$_{121}$ films: (a) random two-phase structure (i.e., sea-and-island structure) developed in the as-cast film; (b) lamellar structure with a wide distribution of orientation developed in the CB-annealed film; (c) lamellar structure with a narrow distribution of orientation developed in the CS_2-annealed film. The size (i.e., correlation length) of domains in the random two-phase structure is denoted with l_p. Long period and lamellar thickness are denoted as L and h (h_{PStFl2} and h_{P2VP}), respectively. Typical I–V curves of the devices fabricated with PStFl2$_7$-*b*-P2VP$_{121}$ films (30 nm thick), which were measured with a compliance current set of 0.01 A: (d, e) as-cast film; (f, g) CB-annealed film; (h, i) CS_2-annealed film. Al top and ITO bottom electrodes were used. The electrode contact area was 0.5 × 0.5 mm^2.

Table 1. Structural Parameters of Nanoscale Films of the PStFl2$_7$-*b*-P2VP$_{121}$ (29/71, v/v) Diblock Copolymer

		random two-phase structure		lamellar structure						
film sample	T (°C)	l_p (nm)[a]	σ_p (nm)[b]	L (nm)[c]	g[d]	h_{PStFl2} (nm)[e]	h_{P2VP} (nm)[f]	$\bar{\varphi}$ (deg.)[g]	σ_φ (deg.)[h]	O_s[i]
as-cast	25	11.8	3.5							
CB-annealed	25			14.6	0.210	5.0	9.6	0	76.0	0.261
CS_2-annealed	25			13.5	0.071	4.6	8.9	0	5.5	0.985
	80			14.1	0.105	4.8	9.3	0	5.5	0.985
	120			14.3	0.112	4.9	9.4	0	7.0	0.976
	130			14.3	0.134	4.9	9.4	0	8.0	0.969
	140			15.0	0.144	5.2	9.8	0	8.0	0.969
	150			15.6	0.148	5.2	10.4	0	7.5	0.972
	160			16.1	0.153	5.5	10.6	0	10.0	0.954
	170			19.5	0.162	6.7	12.8	0	12.5	0.930
	180			20.3	0.162	6.9	13.4	0	13.0	0.925

[a]Domain size of the minor block component. [b]Standard deviation of the domain size of the minor block component. [c]Lamellar long period (*d*-spacing of the lamellar structure). [d]Paracrystal distortion factors of the lamellar structure. [e]Thickness of the PStFl2 lamellae. [f]Thickness of the P2VP lamellae. [g]Mean polar angle between the **n** vector of the lamellar structure and the out-of-plane of the film; for example, $\bar{\varphi}$ is zero when the **n** vector in the film is oriented normal to the film plane. [h]Standard deviation of the polar angle φ. [i]Second-order orientation factor of the lamellar structure.

behavior was confirmed to be well maintained even after six months to one year. $V_{c,ON}$ was +3.0 V during the positive voltage sweep and −4.0 V in the negative voltage sweep, whereas the ON/OFF current ratio fell in the range 10^2–10^5, depending on the reading voltage. On the other hand, the CS_2-annealed film switched on around −4.3 V during a negative voltage sweep but returned to the OFF-state when the power had been turned off (Figure 4h). This switching behavior was found to be repeatable. The ON-state was found to reset to the OFF-state under a reverse voltage sweep. Similar switching behaviors were observed during the positive voltage sweeps, with $V_{c,ON}$ = +3.8 V (Figure 4i). The ON/OFF current ratio was estimated to fall in the range 10^3–10^5, depending on the reading voltage. This unipolar dynamic random access memory

dx.doi.org/10.1021/mz4002113 | ACS Macro Lett. 2013, 2, 555–560

(DRAM) behavior is quite different from the memory behaviors of the as-cast and CB-annealed films.

Representative $I-V$ data for the devices that displayed memory characteristics were further analyzed in detail using a variety of conduction models to investigate their electrical switching characteristics.[9] Logarithmic plots of the $I-V$ data for the devices' OFF-states could be divided into two regimes (Figure S7, Supporting Information). The currents in the first regime (lower voltage regime) for the diblock copolymer films and its PStFl2 homopolymer film could be satisfactorily fitted to an ohmic model, whereas the currents in the second regime were well fit using a trap-limited space-charge limited conduction (SCLC) model. These results collectively indicated that all devices in the OFF-state were governed by a trap-limited SCLC mechanism combined with ohmic conduction. On the other hand, the $I-V$ data for the devices in the ON-state could be satisfactorily fitted using an ohmic conduction model (data not shown).

In view of the electrical switching mechanisms identified above, the charge trapping sites may have originated from the chemical components of the diblock copolymer. As discussed, the P2VP homopolymer displayed dielectric-like characteristics. Thus, all memory behavior originated from the PStFl2 component. The fluorene moiety is an electron donor.[7,8] Thus, a difluorene unit in our polymer can trap holes and stabilize the trapped holes with the aid of the fluorene aromatic rings. The vinyl backbone can act as an electron donor, although it may not have the capacity to stabilize trapped charges alone, given that its hole-trapping capabilities are very weak; however, the electron-donor characteristics of the vinyl backbone could effectively assist the hole trapping and stabilization functions of the difluorene moieties. The chemical structure of the P2VP block included a vinyl moiety and a heteroaromatic pyridine ring per repeating unit, both of which could act as electron donors. Thus, the P2VP block component can potentially assist with hole trapping. The dielectric-like $I-V$ characteristics observed in the P2VP homopolymer films suggested that the P2VP block may not display an appropriate level of hole trapping and stabilization to facilitate electrical memory behavior. Furthermore, the P2VP block formed distinct domains that were separated from the PStFl2 block phase due to the mutual immiscibility of the blocks. Thus, the P2VP domains may contribute either positively or negatively to the hole trapping and transformation in the diblock copolymer films, depending on the morphological structure. Under an applied electrical field, charges may be trapped at trapping sites. The charge trapping sites were expected to be localized at sites distributed throughout the copolymer film layers and were expected to be stabilized to a certain degree. These charge trapping sites acted as stepping stones for charge flow. Thus, under an electric field, local filaments formed via charge trapping sites that enabled current flow through a hopping process and resulted in an ON-state. Furthermore, the energy barriers to hole injection from the electrodes to the diblock copolymer layer (HOMO level) were much lower than the barriers to electron injection from the electrodes to the polymer layer (LUMO level). Therefore, the conduction processes in the devices were dominated by hole injection.

The memory device performances described above depended on nanostructures of the diblock polymer film layer, which varied with the film fabrication conditions. The CB-annealed film displayed WORM memory behavior, as observed in the PStFl2 homopolymer film. Due to the less preferential orientation, some PStFl2 lamellae were aligned along the out-of-plane direction of the film layer (Figure 4b) and, thus, contacted the bottom and top electrodes. Therefore, the observed WORM memory characteristics were attributed to some fraction of the vertically oriented PStFl2 lamellae in contact with both the bottom and top electrode, which created physical routes for charge trapping and transport. The presence of some other fraction of PStFl2 and P2VP lamellae that were oriented along directions rather than the out-of-plane direction of the film contributed to a higher $V_{c,ON}$ and a lower ON-current level than were observed in the PSTFl2 homopolymer film.

By comparison, the CS_2-annealed film that exhibited DRAM behavior displayed a well-defined lamellar structure that was highly oriented along the film plane. In such a confined morphological geometry, charge trapping and stabilization could occur in the PStFl2 lamellae (4.6 nm thick) but could be ineffectual in the dielectric-like P2VP lamellae (8.9 nm thick) (Figure 4c). The P2VP lamellae destabilized the overall charge trapping and transport across the diblock copolymer film layers between the two electrodes, leading to volatile DRAM behavior, which differed significantly from the nonvolatile memory characteristics observed in the CB-annealed film. This result further indicated an important scientific insight that charges can transport across around a 8.9 nm thick P2VP dielectric layer, even under a relatively low applied electric field, 3−5 V.

By contrast, the as-cast film, which exhibited no electrical memory behaviors, formed a sea-and-island structure with a very low population. The PStFl2 block, as the minor component, formed randomly shaped island domains 11.8 nm in size in the dielectric-like P2VP matrix. In view of this morphological characteristic, the dielectric-like $I-V$ characteristics may have resulted mainly from two factors: First, the low population of PStFl2 island domains created long path lengths across the P2VP phases between the PStFl2 islands. Such path lengths across the P2VP phases might be longer than 8.9 nm (that is the thickness of the P2VP lamellae in the CS_2-annealed film). Although the charges became trapped in the PStFl2 domains, it may have been difficult for the charges in one domain to move to another neighboring domain through the dielectric-like P2VP phase. Second, the major portion of the PStFl2 blocks was scattered among the P2VP matrix as individual block chains and/or small aggregates because the phase separation was very limited during the solution coating and subsequent drying process. The small individual PStFl2 block chains and/or aggregates in the dielectric P2VP matrix may not have been able to facilitate charge trapping and transport.

In summary, the PStFl2$_7$-*b*-P2VP$_{121}$ copolymer formed a variety of phase-separated nanostructures in the nanoscale thin films, depending on the film fabrication conditions. Such film morphologies significantly influenced the electrical memory characteristics of the devices; dielectric, WORM memory, and DRAM characteristics were demonstrated. In particular, the DRAM results provided an important insight, that charge transport can occur across the 8.9 nm thick P2VP dielectric layer of a lamellar structure, even under a low electric field. All memory behaviors were governed by a trap-limited SCLC mechanism, combined with ohmic conduction and local filament formation. Overall, PStFl2$_7$-*b*-P2VP$_{121}$ is a suitable active material for devices because it can be produced at low cost and it is amenable to the mass production of high-

dx.doi.org/10.1021/mz4002113 | *ACS Macro Lett.* 2013, 2, 555−560

performance tunable digital memory devices. The memory devices could be operated under very low power consumption levels and displayed excellent unipolar switching with a high ON/OFF current ratio.

■ ASSOCIATED CONTENT

Supporting Information

Materials and thin film preparation, device fabrication, measurements, GIXS data analysis, optical and electrochemical property data, GIXS data, and *I*−*V* data. This material is available free of charge via the Internet at http://pubs.acs.org.

■ AUTHOR INFORMATION

Corresponding Author

*Tel.: +82-54-279-2120. Fax: +82-54-279-3399. E-mail: ree@postech.edu (M. R.). Tel.: +886-2-3366-5236. Fax: +886-2-3366-5237. E-mail: chenwc@ntu.edu.tw (W.-C.C.).

Author Contributions

∥These authors contributed equally to this work.

Notes

The authors declare no competing financial interest.

■ ACKNOWLEDGMENTS

This study was supported by the National Research Foundation (NRF) of Korea (Doyak Program 2011-0028678 and Center for Electro-Photo Behaviors in Advanced Molecular Systems (2010-0001784)) and the Ministry of Education, Science and Technology (MEST) (World Class University Programs (R31-2008-000-10059-0) and BK21 Program). Synchrotron GIXS measurements were supported by MEST, POSCO, and POSTECH Foundation. The work at National Taiwan University was supported by National Science Council under the contract number NSC 98-2221-E-002-006-MY3.

■ REFERENCES

(1) (a) Bates, F. S.; Fredrickson, G. H. *Annu. Rev. Phys. Chem.* **1990**, *41*, 525−557. (b) Fasolka, M. J; Mayes, A. M. *Annu. Rev. Mater. Res.* **2001**, *31*, 323−355. (c) Park, M.; Harrison, C.; Chaikin, P. M.; Register, R. A.; Adamson, D. H. *Science* **1997**, *276*, 1401−1404. (d) Krausch, G.; Magerle, R. *Adv. Mater.* **2002**, *14*, 1579−1583. (e) Jung, J.; Park, H.-W.; Lee, J.; Huang, H.; Chang, T.; Rho, Y.; Ree, M.; Sugimori, H.; Jinnai, H. *Soft Matter* **2011**, *7*, 10424−10428.

(2) (a) Hirao, A.; Watanabe, T.; Ishizu, K.; Ree, M.; Jin, S.; Jin, K. S.; Deffieux, A.; Schappacher, M.; Carlotti, S. *Macromolecules* **2009**, *42*, 682−693. (b) Heo, K.; Yoon, J.; Jin, S.; Kim, J.; Kim, K.-W.; Shin, T. J.; Chung, B.; Chang, T.; Ree, M. *J. Appl. Crystallogr.* **2008**, *41*, 281−291. (c) Jin, S.; Yoon, J.; Heo, K.; Park, H.-W.; Shin, T. J.; Chang, T.; Ree, M. *J. Appl. Crystallogr.* **2007**, *40*, 950−958. (d) Park, I.; Lee, B.; Ryu, J.; Im, K.; Yoon, J.; Ree, M.; Chang, T. *Macromolecules* **2005**, *38*, 10532−10536.

(3) (a) Manners, I. *Angew. Chem., Int. Ed.* **2007**, *46*, 1565−1568. (b) Park, S.; Lee, D. H.; Kim, B.; Hong, S. W.; Jeong, U.; Xu, T.; Russell, T. P. *Science* **2009**, *323*, 1030−1033. (c) Ahn, B.; Hirai, T.; Jin, S.; Rho, Y.; Kim, K.-W.; Kakimoto, M.-a.; Gopalan, P.; Hayakawa, T.; Ree, M. *Macromolecules* **2010**, *43*, 10568−10581. (d) Yoon, J.; Jung, S. Y.; Ahn, B.; Heo, K.; Jin, S.; Iyoda, T.; Yoshida, H.; Ree, M. *J. Phys. Chem. B* **2008**, *112*, 8486−8495.

(4) (a) Hirai, T.; Leolukman, M.; Jin, S.; Goseki, R.; Ishida, Y.; Kakimoto, M.-a.; Hayakawa, T.; Ree, M.; Gopalan, P. *Macromolecules* **2009**, *42*, 8835−8843. (b) Yoon, J.; Jin, S.; Ahn, B.; Rho, Y.; Hirai, T.; Maeda, R.; Hayakawa, T.; Kim, J.; Kim, K.-W.; Ree, M. *Macromolecules* **2008**, *41*, 8778−8784.

(5) (a) Kwon, W.; Rho, Y.; Kamoshida, K.; Kwon, K. H.; Jeong, Y. C.; Kim, J.; Misaka, H.; Shin, T. J.; Kim, J.; Kim, K.-W.; Jin, K. S.; Chang, T.; Kim, H.; Satoh, T.; Kakuchi, T.; Ree, M. *Adv. Funct. Mater.* **2012**, *22*, 5194−5208. (b) Yang, S. Y.; Park, J.; Yoon, J.; Ree, M.; Jang, S. K.; Kim, J. K. *Adv. Funct. Mater.* **2008**, *18*, 1371−1377.

(6) (a) Rubatat, L.; Kong, X.; Jenekhe, S. A.; Ruokolainen, J.; Hojeij, M.; Mezzenga, R. *Macromolecules* **2008**, *41*, 1846−1852. (b) Vriezema, D. M.; Hoogboom, J.; Velonia, K.; Takazawa, K.; Christianen, P. C. M.; Maan, J. C.; Rowan, A. E.; Nolte, R. J. M. *Angew. Chem., Int. Ed.* **2003**, *42*, 772−776.

(7) (a) Li, C.; Hsu, J.-C.; Sugiyama, K.; Hirao, A.; Chen, W.-C.; Mezzenga, R. *Macromolecules* **2009**, *42*, 5793−5801. (b) Sugiyama, K.; Hirao, A.; Hsu, J.-C.; Tung, Y.-C.; Chen, W.-C. *Macromolecules* **2009**, *42*, 4053−4062.

(8) (a) Scherf, U.; List, E. J. W. *Adv. Mater.* **2002**, *14*, 477−487. (b) Gross, M.; Müller, D. C.; Nothofer, H.-G.; Scherf, U.; Neher, D.; Bräuchle, C.; Meerholz, K. *Nature* **2000**, *405*, 661−665. (c) Ranger, M.; Rondeau, D.; Leclerc, M. *Macromolecules* **1997**, *30*, 7686−7691.

(9) (a) Mark, P.; Helfrich, W. *J. Appl. Phys.* **1962**, *33*, 205−215. (b) Campell, A. J.; Bradley, D. D. C.; Lidzey, D. G. *J. Appl. Phys.* **1997**, *82*, 6326−6342. (c) Jessen, K. L. *J. Vac. Sci. Technol. B* **2003**, *21*, 1528−1544. (d) Frenkel, J. *Phys. Rev.* **1938**, *54*, 647−648. (e) Laurent, C.; Kay, E.; Souag, N. *J. Appl. Phys.* **1988**, *64*, 336−343.